E-H mode transition in low-pressure inductively coupled nitrogen-argon and oxygen-argon plasmas

Young Wook Lee, Hye Lan Lee, and T. H. Chung[a)]
Department of Physics, Dong-A University, Busan 604-714, South Korea

(Received 16 January 2011; accepted 23 March 2011; published online 1 June 2011)

This work investigates the characteristics of the E-H mode transition in low-pressure inductively coupled N_2-Ar and O_2-Ar discharges using rf-compensated Langmuir probe measurements and optical emission spectroscopy (OES). As the ICP power increases, the emission intensities from plasma species, the electron density, the electron temperature, and the plasma potential exhibit sudden changes. The Ar content in the gas mixture and total gas pressure have been varied in an attempt to fully characterize the plasma parameters. With these control parameters varying, the changes of the transition threshold power and the electron energy distribution function (EEDF) are explored. In N_2-Ar and O_2-Ar discharges at low-pressures of several millitorr, the transition thresholds are observed to decrease with Ar content and pressure. It is observed that in N_2-Ar plasmas during the transition, the shape of the EEDF changes from an unusual distribution with a flat hole near the electron energy of 3 eV in the E mode to a Maxwellian distribution in the H mode. However, in O_2 -Ar plasmas, the EEDFs in the E mode at low Ar contents show roughly bi-Maxwellian distributions, while the EEDFs in the H mode are observed to be nearly Maxwellian. In the E and H modes of O_2-Ar discharges, the dissociation fraction of O_2 molecules is estimated using optical emission actinometry. During the E-H mode transition, the dissociation fraction of molecules is also enhanced. © *2011 American Institute of Physics*.
[doi:10.1063/1.3587156]

I. INTRODUCTION

In plasma processing, molecular and mixture gases are used in practice in order to achieve the desired selectivity and to improve the etch rate. Oxygen discharges are widely used for industrial-materials processing, such as dry etching of a photoresist, formation of an oxide film, and ashing of samples.[1,2] Oxygen with a mixture of rare gases is usually used as the primary gas for oxidization, formation of passivation layer, or other plasma technologies applied to the production of integrated circuits. The etching of SiO_2 and Si typically involves mixtures of Ar and O_2 with the addition of a fluorocarbon.[3,4] Nitrogen discharges in a mixture of dilution gases as well as pure nitrogen discharges have been employed in a variety of material processing applications.[5–8] The atomic nitrogen and oxygen play a key role in the processes such as etching and synthesis of nitrides and oxides, thus making the concentration of atomic species in the molecular gas plasma a significant concern.[9,10] The determination of the radical atom densities as a function of power and pressure is essential in the understanding and optimization of the plasma process for micro-electronics materials.

Recently there has been a steadily growing interest in inductively coupled plasma (ICP) sources for numerous plasma-enhanced materials processing because the ICP sources provide stable, reproducible, and highly uniform high density plasmas. ICP has two sustaining modes according to the plasma external condition, such as input power, gas pressure, etc.[11–14] One is the inductive H mode, where high density plasma is generated by electromagnetic field. The other is called the capacitive E mode, where plasma is ignited by static electric field between segments of a current coil. The capacitive discharge mode of the ICP results in the observable properties of faint light emission, relatively low plasma density, and high plasma potential.[15,16] With increasing the rf power, an E-to-H transition occurs, and then the intensity of the OES signal increases markedly, while the coil current drops.[17–20] High plasma density with an abrupt jump of the plasma density, bright light emission, and low plasma potential are well-known main characteristics of the H mode. These sudden changes, such as the light emission, the plasma density, and the plasma potential, demonstrate the discharge power coupling transition from the capacitive mode (E mode) to the inductive mode (H mode).

It has been known that most of molecular N_2-Ar and O_2-Ar ICP discharges are characterized by high neutral atom content.[7] This paper is concerned with the E-H mode transition of N_2 -Ar and O_2-Ar ICP discharges. In order to characterize the transition, the important plasma parameters that should be observed are the electron density, electron temperature, plasma potential, optical emission intensities from plasma species, and electron energy distribution function (EEDF). The convenient methods to measure these quantities include the Langmuir probe technique and optical emission spectroscopy. Depending on the applications, the Ar content in the mixture can vary from less than a few percent to over 90% (Ar-dominated discharge). The gas pressure is also dependent on the application and the size of ICP chamber and rf antenna. With these control parameters varying, the changes of the transition threshold power and the EEDF are explored. The purpose of this work is to characterize the

[a)]Author to whom correspondence should be addressed. Electronic mail: thchung@dau.ac.kr.

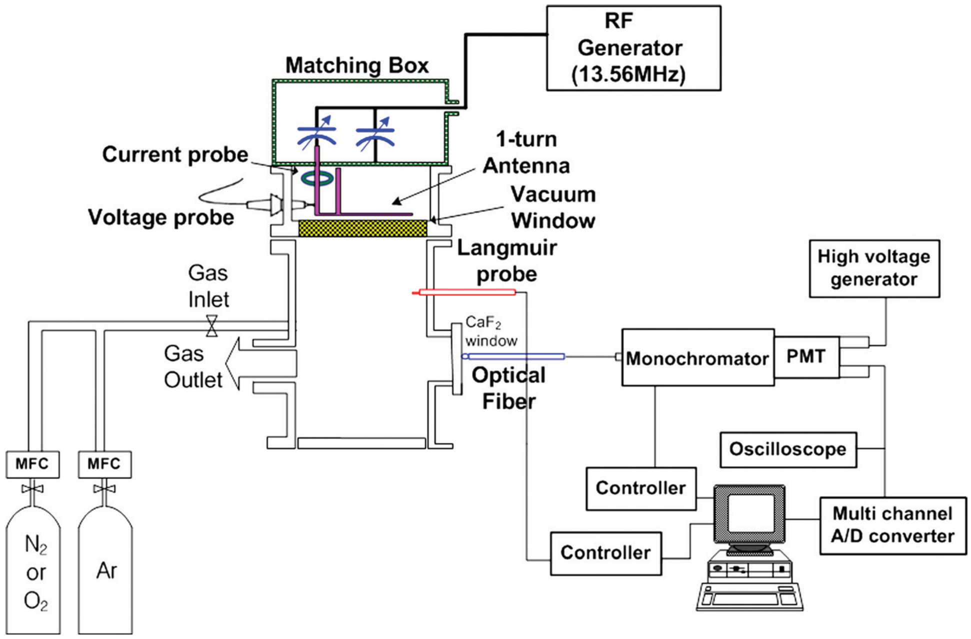

FIG. 1. (Color online) Schematic diagram of experimental setup and diagnostics system.

properties of the E-H mode transition in inductively coupled N_2-Ar and O_2-Ar discharges with varying operating parameters. The operating parameters, such as the Ar content in the gas mixture and total gas pressure, have been varied in an attempt to fully characterize plasma parameters. Also, in E and H modes, the density of neutral atom is estimated by using optical emission actinometry.

II. EXPERIMENT

A schematic diagram of the experimental setup with the diagnostics system (optical emission spectroscopy (OES) and Langmuir probe) is shown in Fig. 1. The plasma chamber consists of a stainless-steel cylinder with a 28-cm diameter and a 34-cm length. A 1.9-cm-thick by 27-cm-diameter tempered glass plate mounted on one end separates the planar one-turn induction coil from the plasma. The induction coil is made of copper (with water-cooling) and is connected to an L-type capacitive matching network and an rf power generator.

The plasma chamber is evacuated by using a diffusion pump backed by rotary pump giving a base pressure of 5×10^{-6} Torr. The equilibrium gas pressure in the chamber is monitored with a combination vacuum gauge (IMG 300). The source gases are N_2 and O_2. The argon is introduced as an adding gas. The Ar content in the gas mixture is varied in the range of 5-80%. The operating gas pressure is controlled by adjusting the mass flow controller and varied in the range of 1-5 mTorr. A 13.56 MHz generator (ENI OEM 12) drives an rf current in a flat one-turn coil through the rf power generator and matching network. Because of the circulating currents in the antenna coil and matching system, the ICP power absorbed into the plasma can be obtained by $P_{ICP} = P_{rf} - I^2R_c$. Here I is the rms current, P_{rf} is the input rf power, and R_c is the circuit resistance of antenna and matching system. Calculated R_c in our system is 0.17 Ω.

Light collection was made by the optical fiber (0.1 mm slit diameter) attached to the CaF_2 window. The light intensity of emissive molecules and radicals in the plasma was focused by means of optical fiber into entrance slit of 0.75 m monochromator (SPEX 1702), equipped with a grating of 1200 grooves per millimeter and slit width of 100 μm. The light was collimated at the exit slit where a photomultiplier tube converted photons into an electric signal. Optical emission spectra were recorded in the wavelength range of 250–850 nm with a resolution of 0.1 nm. The measured emission spectra should be corrected for the spectral response of the detection system, which includes optical fiber, monochromator, and photomultiplier tube. The detection system had to be calibrated in intensity using a quartz halogen lamp with a known spectral radiance.

An rf-compensated cylindrical single Langmuir probe was mounted through one of the ports on the vacuum chamber. The probe tip made of tungsten with a diameter of 0.1 mm and a length of 10 mm is used to measure the plasma parameters. The probe tip was located on the axis of the cylinder at 14 cm below the tempered glass plate. Probe circuit resistance is accounted for by the use of the reference ring probe with a resonance filter that reduces the rf distortion of probe characteristics. To measure the plasma parameters, the harmonic technique, which exploits the generation of harmonics resulting from excitation of the nonlinearity of the single Langmuir probe characteristics, combined with Druyvesteyn method was used. In the harmonic method,[21] the voltage applied to the probe consists of the sweep voltage and the sinusoidal voltage v_0 of the frequency ω. The second harmonic term $I_{2\omega}$ of the measured probe current is proportional to the second derivative as $I_{2\omega} \approx (1/4)v_0^2 d^2I/dV^2 \cos 2\omega t$, which is related to the electron energy distribution function (EEDF), $f(\epsilon)$,

$$f(\epsilon) = \frac{2m}{e^2 S}\left(\frac{2eV}{m}\right)^{1/2}\frac{d^2 I}{dV^2}, \tag{1}$$

where e is the electron charge, S is the probe area, m is the mass of electron, V is the probe potential referenced to the plasma potential (V_p), and ϵ is measured in units of electron volts. The electron density (n_e) and the effective electron temperature (T_e) are calculated with the measured EEDF as follows:

$$n_e = \int_0^{\epsilon_{max}} f(\epsilon)d\epsilon, \quad T_e = \frac{2}{3n_e}\int_0^{\epsilon_{max}} \epsilon f(\epsilon)d\epsilon, \quad (2)$$

where ϵ_{max} is determined by the dynamic range of the EEDF measurement. The electron temperature can also be determined from the slope of the probe *I-V* curve in the exponential region (from the point where the probe current is zero to where the slope of the curve begins to decrease). We observed that both methods yield almost same values of the electron temperature.

III. SPATIALLY AVERAGED MODEL

To explore the characteristics of the E-H mode transition in inductively coupled N_2-Ar and O_2-Ar discharges, a simple model can be utilized. Global models indicate that the electron temperature in a discharge is determined predominantly by particle balance, whereas power balance determines the electron density. For a stable E or H discharge mode to exist, the power absorbed by the electrons, P_{abs}, must identically balance the power dissipated P_{diss}. If the energy lost per ionization is fixed, the power dissipated by the plasma electrons varies linearly with the electron density n_e. A simple linear relation between P_{diss} and n_e should, in principle, hold for both an E- and H-mode discharge.[18] Particle and power balances in N_2-Ar and O_2-Ar discharges can be expressed in a spatially averaged form in the steady state.[5,22] The particle balance equation is written as

$$\left(k_{iz}^{X_2} n_e[\mathrm{X_2}] + k_{iz}^{X} n_e[\mathrm{X}] + k_{iz}^{Ar} n_e[\mathrm{Ar}]\right)V = (2\pi R^2 h_l + 2\pi RLh_R)n_e u_B, \quad (\mathrm{X = N\ or\ O}), \quad (3)$$

where R, L, and V are the radius, the height, and the volume of the cylindrical chamber, respectively. Here $k_{iz}^{X_2}$, k_{iz}^{X}, and k_{iz}^{Ar} denote the rate coefficients of the electron impact ionization of X_2, X, and Ar, respectively, and u_B is the Bohm velocity. All positive ion species are assumed to have the same u_B corresponding to an effective ion mass. The factors h_l and h_R are the edge to center positive ion density ratios in the axial and radial direction given as[23]

$$h_l = \frac{0.86}{\sqrt{3+\frac{L}{2\lambda_i}}}, \quad h_R = \frac{0.8}{\sqrt{4+\frac{R}{\lambda_i}}}, \quad (4)$$

where λ_i is the ion mean free path in X_2-Ar plasma given by

$$\frac{1}{\lambda_i} = [\mathrm{Ar}]\sigma_{\mathrm{Ar}} + [\mathrm{X_2}]\sigma_{\mathrm{X_2}} + [\mathrm{X}]\sigma_{\mathrm{X}}, \quad (5)$$

where $\sigma_{\mathrm{Ar}}, \sigma_{\mathrm{X_2}}, \sigma_{\mathrm{X}}$ are the total ion-neutral collision cross sections

Rearranging Eq. (3), we have

$$k_{iz}^{X_2}[\mathrm{X_2}] + k_{iz}^{X}[\mathrm{X}] + k_{iz}^{Ar}[\mathrm{Ar}] = \frac{u_B}{d_{eff}}, \quad (6)$$

where d_{eff} is the effective length $(= RL/2(Rh_l + Lh_R))$. It should be noted that as the Ar content increases, λ_i is decreased. This causes the h_l and h_R factors to decrease, thus making d_{eff} increase, which results in a slight decrease in T_e (assuming the Arrhenius forms of k_{iz}).

The mode transition threshold is obtained from the balance of powers absorbed by the plasma from the external rf field, P_{abs}, and dissipated for maintenance of major elementary processes in a discharge, P_{diss}, including electron impact ionization, associative ionization, excitation/deexcitation of higher atomic/molecular levels through electron impact and heavy particle collision processes, escaping of positive ions to the discharge walls through the sheaths to the walls, and thermal motion. The dissipated power is expressed as

$$P_{diss} = e\varepsilon_c^{X_2} k_{iz}^{X_2} n_e[\mathrm{X_2}]V + e\varepsilon_c^{X} k_{iz}^{X} n_e[\mathrm{X}]V + e\varepsilon_c^{Ar} k_{iz}^{Ar} n_e[\mathrm{Ar}]V + e(\varepsilon_e + \varepsilon_i)n_e u_B A_{eff}, \quad (7)$$

where $A_{eff}(= V/d_{eff})$ is the effective surface area of the chamber. The collisional energy loss per electron-ion pair created ε_c represents the power loss due to elastic and inelastic collisions, which includes all excitation energies such as vibrational, dissociative, and electronic excitations. Here $\varepsilon_c^{X_2}$ and ε_c^{X} are the collisional energy loss per ionization event of molecule and atom, respectively, and ε_c^{Ar} is the collisional electron energy loss per ionization event of argon gas. The average energy of escaping ions, ε_i, is the sum of the ion energy entering the sheath $(T_e/2)$ and the energy gained in the sheath V_{sh} (sheath voltage drop), and ε_e is the average energy of electrons escaping to the walls and is assumed to be equal to $2T_e$. In Fig. 2, the calculated collisional energy losses per electron-ion pair created, ε_c, are plotted as a function of T_e for the ground state molecules, N_2 and O_2, and the ground state atoms (N, O, Ar), when assuming a Maxwellian electron energy distribution.[22,24] We note that electron collisional inelastic loss rates in nitrogen and oxygen are higher than in argon.

The stable operating points in density n_e for the E- and H-modes of the plasma can then be found by equating

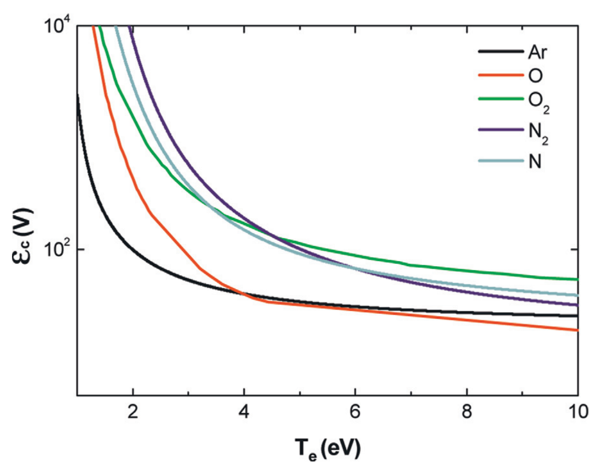

FIG. 2. (Color online) The collisional energy loss per electron-ion pair created, ε_c, as a function of T_e for the ground state molecules (N_2 and O_2) and the ground state atoms (N, O, Ar) from Refs. 22 and 24. Reprinted with permission from E. G. Thorsteinsson and J. T. Gudmundsson, Plasma Sources Sci. Technol. 18, 045001 (2009) and J. T. Gudmundsson, T. Kimura, and M. A. Lieberman, Plasma Sources Sci. Technol. 8 22 (1999). Copyright © 1999 and 2009, IOP Science.

absorbed and dissipated power. Combining Eqs. (6) and (7), we have

$$n_e = \frac{P_{abs}}{eu_B A_{eff}\left(\varepsilon_c^{X_2}\delta_{X_2} + \varepsilon_c^{X}\delta_{X} + \varepsilon_c^{Ar}\delta_{Ar} + \varepsilon_e + \varepsilon_i\right)}, \quad (8)$$

where $\delta_{X_2} = n_{X_2^+}/n_e, \delta_X = n_{X^+}/n_e, \delta_{Ar} = n_{Ar^+}/n_e$. As the Ar content increases, the term $\varepsilon_c^{X_2}\delta_{X_2} + \varepsilon_c^{X}\delta_{X} + \varepsilon_c^{Ar}\delta_{Ar}$ decreases because $\varepsilon_c^{X_2}$ and ε_c^{X} are several times larger than ε_c^{Ar} at $T_e = 3-5$ eV.[22,24] The total energy loss per electron-ion pair is written as

$$\varepsilon_T = \varepsilon_c^{X_2}\delta_{X_2} + \varepsilon_c^{X}\delta_{X} + \varepsilon_c^{Ar}\delta_{Ar} + \varepsilon_e + \varepsilon_i. \quad (9)$$

As shown in Fig. 2, $\varepsilon_c^{X_2} \gg \varepsilon_c^{Ar}$ in the T_e range of 2–5 eV in this study, hence ε_T is expected to decrease with the Ar content. Ku *et al.*[25] obtained the total energy losses experimentally from the power balance equation $P_{abs} = e\varepsilon_T A_{eff}\Gamma_+$ (Γ_+ is ion flux) and demonstrated that in the case of Ar mixture plasma with molecular gas, the total energy loss decreased with fractional Ar flow rate. Therefore for a fixed power, n_e increases with increased Ar content, and for a fixed n_e, as ε_T is decreased, the transition threshold power is expected to decrease. This implies that the transition threshold power decreases with increasing Ar content. The pressure dependence of ε_T in molecular discharges is very complex because each term in Eq. (9) depends on pressure in complicated ways.

IV. RESULTS AND DISCUSSION

Figure 3 shows the changes of n_e with ICP power at 1.4 mTorr for different Ar contents in N_2-Ar ICP discharges. Mode transition and hysteresis is often illustrated in terms of the electron density with respect to the applied rf power to the antenna coil. Increasing the rf power shifts the discharge from capacitive mode through a capacitive inductive transition, mixed E-H regime, which finally jumps into inductive mode. In inductive H mode, the electron density jumps by almost two orders of magnitude.[16] The sudden changes demonstrate the discharge power coupling transition from the E mode to the H mode. Note that the transition threshold power in the pure N_2 gas discharge at 1.4 mTorr is 260 W, which is much higher than the transition power 150 W in the case of argon discharge under the same reactor. This may be due to a larger energy loss for the molecular gas through vibrational/rotational excitations and dissociation collisions as mentioned before. As expected, the mode transition threshold is observed to decrease with the Ar content (from 230 W (Ar 5%) to 160 W (Ar 80%)). Because the rates of inelastic collisions in nitrogen increase with decreasing Ar content with relative effects of quenching of excited molecular states naturally leading to an increase in the discharge maintenance fields and thus mode transition thresholds. In the low-pressure region of this work, the hysteresis was not observed.[14] In the H mode, with an increase in the Ar content, n_e increases in agreement of the discussions in Sec. III. Although not shown, as usual T_e decreases with pressure and increases slightly with power. The measurements show an increase in T_e as power increases for most of the cases. This is evidence of neutral heating because a higher neutral temperature at constant gas pressure implies a decrease in neutral gas density, which results in an increase in T_e.[26] This trend is in agreement with the modeling and the experimental work.[22,27]

Figure 4 represents the changes of n_e with ICP power at 1.1 mTorr for different Ar contents in O_2-Ar ICP discharges. Note that the transition threshold power in the pure O_2 gas discharge at 1.1 mTorr is 250 W. The mode transition threshold is observed to decrease with the Ar content (from 210 W (Ar 5%) to 160 W (Ar 80%)). Similar to the case of N_2-Ar plasma, n_e increases and T_e slightly increases with the Ar content; this is in agreement of the result by Lee *et al.*[28] At the power of 300 W, n_e is in the range of $4-5\times10^9 \text{cm}^{-3}$, a little larger than those in N_2-Ar plasma at the same power. This is because N_2-Ar plasma has a larger ε_T than O_2-Ar plasma in Eq. (8).

The transition threshold power also depends on pressure. The theoretical calculations show that the transition coil current becomes minimal when the electron-neutral collision frequency coincides with the angular frequency of the rf power.[14] For an argon gas, this is satisfied at about 25 mTorr argon pressure with 13.56 MHz rf power. Because this work concerns lower pressure than 25 mTorr, the transition power decreases with pressure. In pure argon plasmas, the transition thresholds diminish with increasing pressure. Although not shown in the figure, the transition thresholds are observed to be 150 W (1 mTorr), 130 W (6 mTorr), and 100 W (7.5 mTorr). It has been understood that ion mobility

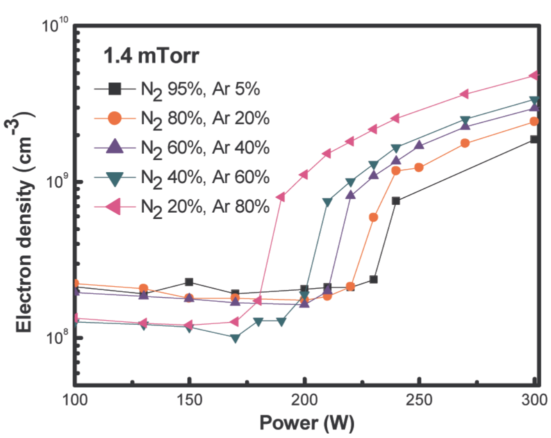

FIG. 3. (Color online) Changes of electron density with ICP power at 1.4 mTorr for different Ar contents in N_2-Ar ICP discharges.

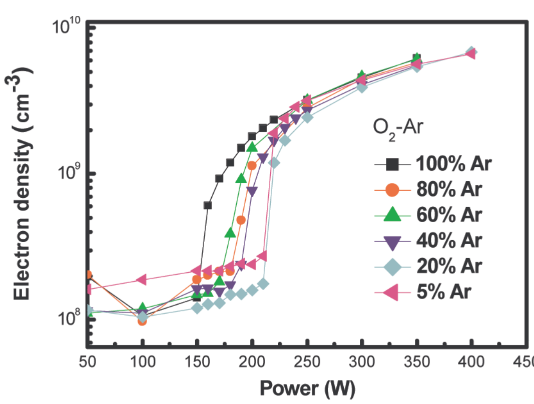

FIG. 4. (Color online) Changes of electron density with ICP power at 1.1 mTorr for different Ar contents in O_2-Ar ICP discharges.

decreases with pressure; this results in the depletion of ions to the chamber walls and in excessive rf power, which is typically proportional to the plasma density. Thus the discharge in argon can be sustained at elevated pressures with lower input powers.[20] On the contrary, the transition threshold for molecular gas discharges is thought to increase with pressure. The general understanding is that the rates of inelastic collisions in molecules increase with pressure with the relative effects of quenching of excited molecular states naturally leading to an increase in the discharge maintenance fields and thus mode transition thresholds.[20]

Figure 5(a) represents the evolution of n_e with ICP power for different pressures in $N_2 - 80\%$ Ar plasma. At a pressure of 1.4 mTorr, the transition from E to H mode occurs smoothly, whereas at higher pressures, it occurs suddenly.[11] Figures 5(b) and 5(c) show the changes of n_e and V_p with ICP power for different pressures and Ar contents in O_2-Ar plasma. The high plasma potential in the E mode is caused by the capacitive power coupling, and its sudden drop when the mode transition occurs implies an entire change in the power coupling.[13] Figures 5(b) and 5(c) also indicate that the transition thresholds appear consistently in the variations of n_e and V_p. In the mixture plasmas at low pressures shown in Fig. 5, the transition thresholds are decreased with increased pressure, indicating that the role of "argon" effects dominates. One reason for this may be that the experiments are performed at Ar-rich mixtures. This can also be accounted for because the transition threshold is related to the breakdown voltage. The operating voltage of the ICP employed in this work lies in the left side of the Paschen minimum. Therefore an increase of pressure results in lowering the breakdown voltage, and the transition occurs at lower power. Thus at 1.4 mTorr for N_2-Ar plasma (and 1.1 mTorr for O_2-Ar plasma), more ICP power is required for a sufficient plasma density in order to sustain the H mode than at 3 mTorr.

Figure 6 shows the electron energy probability functions (EEPFs) at the pressure of 1.4 mTorr. Figure 6(a) is EEPFs in the E mode (at the ICP power of 130 W), and 6(b) is EEPFs in the H mode (at the ICP power of 300 W) of N_2-Ar ICP discharges for different Ar contents. The EEPFs in the E mode have an unusual distribution with a flat hole near the electron energy of 3 eV. The shape of the EEPF in the E

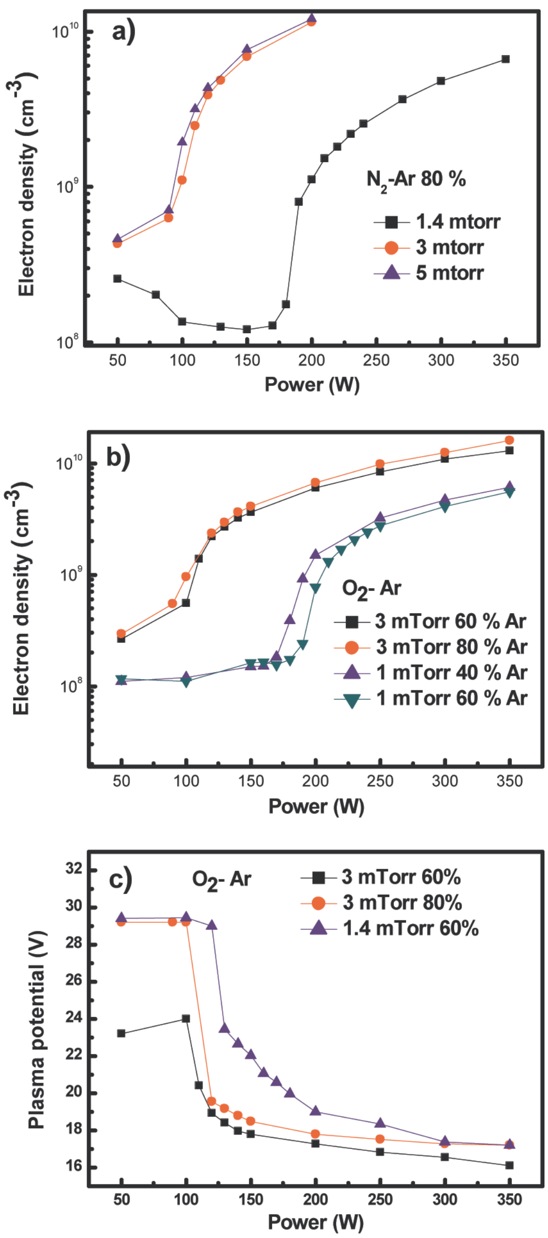

FIG. 5. (Color online) Changes of the transition threshold power with pressure: (a) n_e in N_2-Ar ICP discharges, (b) n_e, and (c) V_p in O_2-Ar ICP discharges.

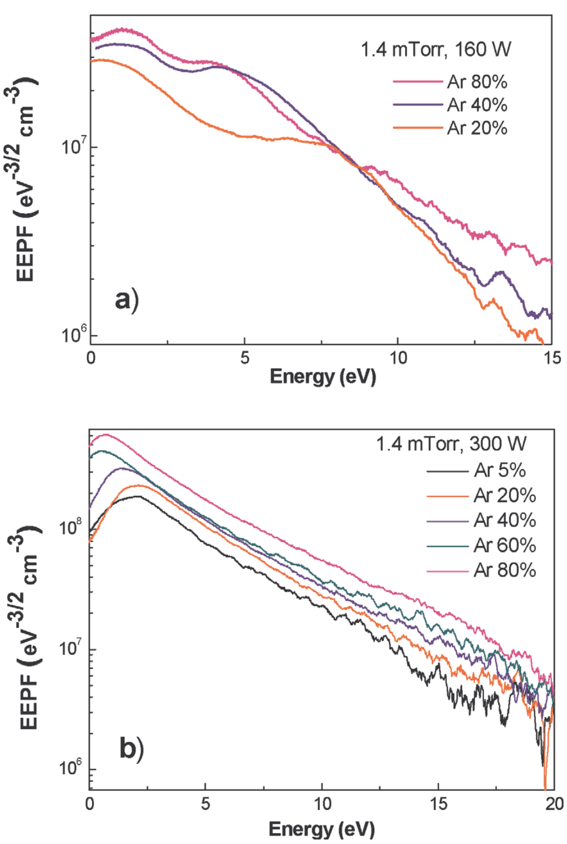

FIG. 6. (Color online) Electron energy probability functions (EEPFs) (a) in the E mode (at the ICP power of 130 W) and (b) in the H mode of N_2-Ar ICP discharges at the pressure of 1.4 mTorr for different Ar contents (ICP power of 300 W).

mode retains the characteristics of the vibrational excitation collisions between electrons and molecules. This is closely related to electron kinetics and electron energy relaxation length.[29] The collision cross section for the vibrational excitation sharply peaks at this electron energy of 3 eV. This indicates that these electrons participate mainly in resonant electron-molecule vibrational excitation collisions, and the electron energy relaxation lengths become shorter in the energy range where the vibrational cross section is large. Electrons participating in the vibrational excitation collisions become very slow, and the EEPF at the center of the discharge has a deep hole near 3 eV.[29] As the nitrogen fraction is increased, the electron energy relaxation lengths decrease, thus this tendency is more clearly shown. When the transition from E mode to H mode occurs, the EEPF evolves into a Maxwellian distribution and the hole disappears. This evolution of the EEPF can be explained by the occurrence of electron energy thermalization resulting from the electron-electron collision effect, and it occurs when the electron-electron collision time becomes shorter than the electron residence time.[29] The distributions in the H mode are observed to be approximately Maxwellian at any Ar content. The EEPFs show that the electron density increases with ICP power and Ar content. The number of high-energy electrons are observed to increase with the Ar content and with increasing ICP power. These electrons may contribute to an increase in the electron-impact dissociation. Moreover, although not shown in the figure, the shape of the normalized EEPF in the H mode is independent of the increasing power; this explains why there is no alteration in the power coupling mechanism to the electrons.[15,16]

Figures 7(a) and 7(b) represent the EEPFs for different Ar contents in the E mode (at the power of 140 W) and in the H mode (at the power of 300 W), respectively, of O_2-Ar ICP discharges at the pressure of 1.1 mTorr. The EEPFs in the E mode at low Ar contents show roughly bi-Maxwellian distributions. But the EEPF for the Ar 60% becomes Maxwellian. In the H mode, the EEPFs are observed to be nearly Maxwellian. The Ar-dominating plasma is more Maxwellian and noise-free. For most of the mixture plasmas in the E mode, the population of electrons with high energy exhibits an unstable behavior, which might be caused by noise. Also, the easy heating due to a frequent electron-impact rovibrational excitations of nitrogen molecules is thought to contribute to the fluctuation of the probe currents. In the E mode, the EEPFs are close to bi-Maxwellian distributions. These are the characteristic of a capacitively coupled plasma that appears due to the two electron heating mechanisms involved; the stochastic heating adjacent to the sheath, and the ohmic heating in the plasma bulk. In the H mode, reduced plasma potential indicates low voltages involved in the plasma, and, hence, the EEPF measurements are less perturbed by the rf distortions. The EEPF evolution with increasing ICP power and particularly in the vicinity of the E to H mode transitional region is noticeable. In an argon plasma with the pressure range of 8-15 mTorr, the proportion of low energy electrons ($\epsilon < 4$ eV) considerably decreased while the proportion of high energy electrons ($\epsilon > 4$ eV) increased as the discharge moves from E mode to H mode.[14]

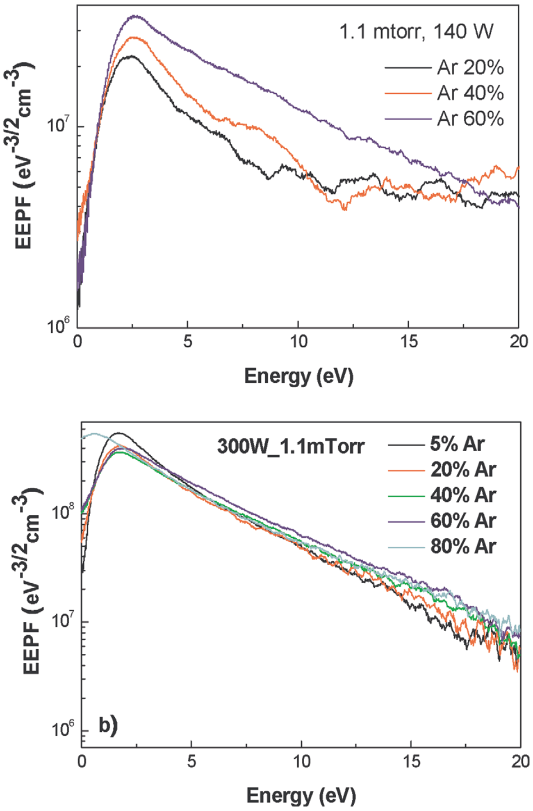

FIG. 7. (Color online) Electron energy probability functions (EEPFs) for different Ar contents (a) in the E mode (at the ICP power of 140 W) and (b) in the H mode (ICP power 300 W) of O_2-Ar ICP discharges at the pressure of 1.1 mTorr.

The transition from a bi-Maxwellian distribution function at lower powers to a Maxwellian distribution at higher powers is due to the shielding of the electrostatic field by reducing electrostatic stochastic heating and high electron-electron collision frequency as a result of an increase in n_e with increasing power[29] in good agreement with the argument developed previously (150 mTorr).[18] The presence of the overpopulated low-energy electron group is being referred to the stochastic heating in the developed oscillating sheath and by the nonlocal electron kinetics in the low-pressure discharge conditions.[30,31]

In order to observe a sudden change in the intensity of the light emission from plasma species, several spectral band or lines are chosen; 337.1 nm from the second positive system of N_2 ($C^3\Pi_u(0) \rightarrow B^3\Pi_g(0)$), 391.4 nm from the first negative system of N_2^+ ($B^2\Sigma_u^+(0) \rightarrow X^2\Sigma_g^+(0)$), 777.4 nm from O ($2p^{3\,5}P \rightarrow 2p^{3\,5}S$), 844.6 nm from O ($2p^{3\,3}P \rightarrow 2p^{3\,3}S$), 750.4 nm from Ar ($2p_1 \rightarrow 1s_2$), and 811.5 nm from Ar ($2p_9 \rightarrow 1s_5$). Figures 8(a) to 8(d) represent the changes of the optical emission intensities from N_2 337.1 nm, N_2^+ 391.4 nm, Ar 750.4 nm, and Ar 811.5 nm, respectively, with power in the N_2-Ar ICP discharges at $p = 1.4$ mTorr. The transition thresholds where a sudden jump in emission intensity occurs are a little larger than those in n_e (Fig. 3), but the trend agrees well with the evolution of n_e. The increase in the intensity of the 391.4 nm line is relatively smooth, implying that the change in the electron impact excitation rate of N_2^+ is not abrupt during the mode transition. Because the excitation energy of the N_2^+

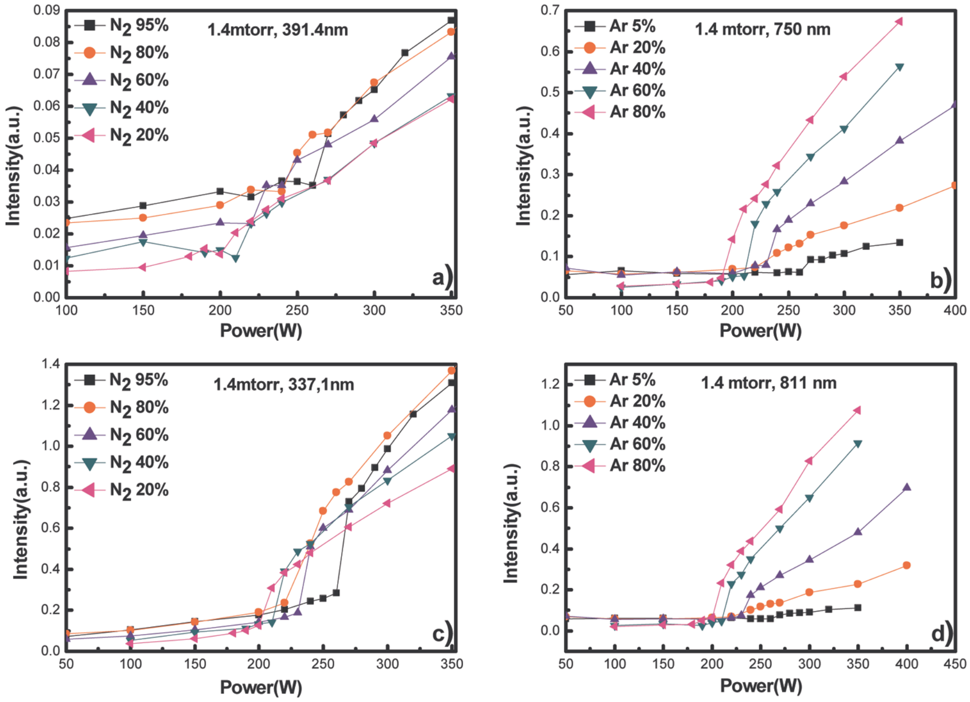

FIG. 8. (Color online) Changes of the optical emission intensities from (a) the second positive system of N_2 $(C^3\Pi_u(0) \rightarrow B^3\Pi_g(0))$ 337.1 nm, (b) first negative system of N_2^+ 391.4 nm, (c) Ar 750.4 nm $(2p_1 \rightarrow 1s_2)$, and (d) Ar 811.5 nm $(2p_9 \rightarrow 1s_5)$ with power in the N_2-Ar ICP discharges at $p = 1.4$ mTorr.

391.4 nm line is higher than that of the N_2 337.1 nm line, the electron energy plays an important role in determining the emission intensities. A drop in T_e during the mode transition contributes to the smooth variation of the N_2^+ 391.4 nm line. It should be noted that there exists a considerable amount of step-wise excitation of molecular and ionized nitrogen due to very weak collisional quenching of excited states by N_2 and Ar due to low pressure region. Figures 9(a) to 9(d) show the changes of the optical emission intensities from O 777.4 nm, O 844.6 nm, Ar 750.4 nm, and Ar 811.5 nm, respectively, with power in the O_2-Ar ICP discharges at $p = 1.1$ mTorr. Also we observe a similar trend to that in Fig. 4. The increases in the intensities are mainly caused by the n_e jump during the mode transition. Although T_e decreases in the transition, the excitation rates of O and Ar to higher level are less influenced by T_e in the range of 5–8 eV.

Figure 10(a) represents the intensity ratio $I_{844.6}/I_{750.4}$ as a function of power for the Ar content 5% at the pressure of 1.1 mTorr. Using actinometry, the dissociation fraction of O_2 can be calculated as[32]

$$\frac{[O]}{[O_2]} = \frac{K_{750}}{K_{844}} \frac{\nu_{750}}{\nu_{844}} \frac{A_{750}}{A_{844}} \frac{\tau_{750}}{\tau_{844}} \frac{k_{Ar}^{dir}}{k_e^{3P}} \frac{[Ar]}{[O_2]} \frac{I_{844}}{I_{750}} - \frac{k_{de}^{3P}}{k_e^{3P}}, \quad (10)$$

where K is a factor depending on plasma volume, solid angle, and spectral response of the spectrometer, ν is the

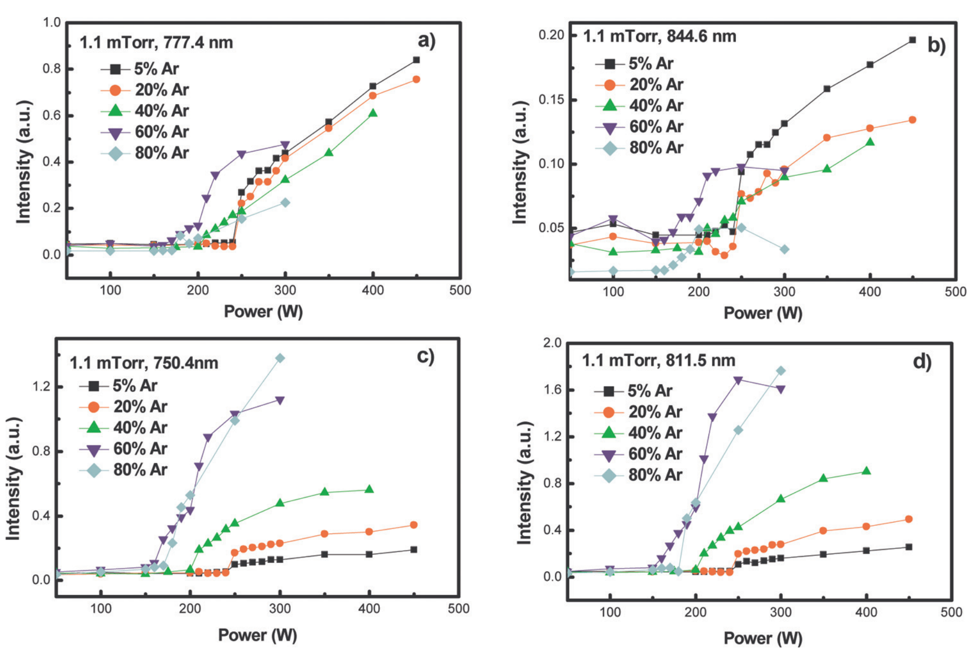

FIG. 9. (Color online) Changes of the optical emission intensities from (a) O 777.4 nm $(2p^3\,{}^5P \rightarrow 2p^3\,{}^5S)$, (b) O 844.6 nm $(2p^3\,{}^3P \rightarrow 2p^3\,{}^3S)$, (c) Ar 750.4 nm $(2p_1 \rightarrow 1s_2)$, and (d) Ar 811.5 nm $(2p_9 \rightarrow 1s_5)$ with power in the O_2-Ar ICP discharges at $p = 1.1$ mTorr.

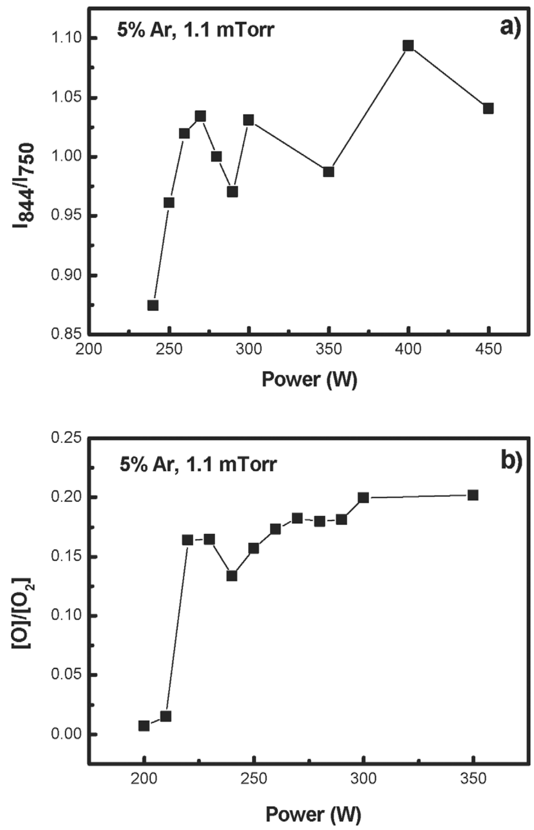

FIG. 10. (a) Intensity ratio $I_{844.6}/I_{750.4}$ as a function of ICP power for the Ar content 5% at the pressure of 1.1 mTorr. (b) Calculated dissociation fraction of oxygen molecules as a function of ICP power.

frequency of the transition, τ is the lifetime of the excited state, and A is the optical emission probability for the transition. Here k_{Ar}^{dir} is the rate coefficient for electronic excitation to $2p_1$ of the ground state Ar, k_e^{3P} is the rate coefficient for electron-impact direct excitation to $O(2p^3\,{}^3P)$ from the ground-state O, and k_{de}^{3P} is the rate coefficient for electron-impact dissociative excitation to $O(2p^3\,{}^3P)$ from the ground-state O_2.

Based on the actinometry, the dissociation fraction of oxygen molecules is calculated as a function of power as shown in Fig. 10(b). For Ar 5% discharge at 1.1 mTorr, the dissociation fraction is increased from 0.007 (E mode) to 0.17 (H mode) in the transition region. It should be noted that an enhancement of oxygen atom density is associated with an enhancement in the electron density (with higher energy), but a decrease in T_e is not necessarily associated with a decrease in the dissociation fraction.[9] From the global balance of the discharge kinetics, the dissociated neutral atom density is expected to be proportional to the power.[33] This is also confirmed in the figure. The trend of change in the dissociation fraction correlates well with the electron density and the electron energy probability function.

V. CONCLUSION

The investigation of E-H mode transitions in low-pressure inductively coupled N_2-Ar and O_2-Ar plasmas was performed using OES and Langmuir probe measurement under the conditions of gas pressures in the range of 1-5 mTorr. The transitions from E to H mode with variation of Ar content and operating gas pressure have been demonstrated. The sudden changes, such as the light emission, the electron density, and the plasma potential, demonstrate the discharge power coupling transition from E to H mode. The transition thresholds are decreased with the Ar content and increased pressure. With increasing Ar content, the electron density is found to increase and the electron temperature to slightly decrease. All these observations can be explained by a spatially averaged global model of mixture plasmas. It is observed that in N_2-Ar plasmas during the transition, the shape of the EEDF changes with a switch from an unusual distribution with a flat hole near the electron energy of 3 eV in the E mode to a Maxwellian distribution in the H mode. However, in O_2-Ar plasmas, the EEDFs in the E mode at low Ar contents show roughly bi-Maxwellian distributions, while the EEDFs in the H mode are observed to be nearly Maxwellian. During the E-H mode transition, the dissociation fraction of molecules is also enhanced. In the H mode, the dissociation fraction increases with ICP power as expected.

ACKNOWLEDGMENTS

The authors are grateful to Dr. Jon Gudmundsson of University of Iceland for providing the electron collisional energy loss data and to Prof. C. W. Chung of Hanyang University for valuable discussions. This work was supported by the National Research Foundation of Korea (NRF) funded by the Ministry of Education, Science, and Technology (Grant No 20090082669, Fusion Core Research Center Program).

[1]D. L. Flamm, Plasma Chem. Plasma Process. **1**, 37 (1981).
[2]A. Granier, F. Nicolazo, C. Vall'ee, A. Goullet, G. Turban, and B. Grolleau, Plasma Sources Sci. Technol. **6**, 147 (1997).
[3]T. Sato and T. Makabe, J. Appl. Phys. **98**, 113304 (2005).
[4]Y. Hayashi, S. Hirao, Y. Zhang, T. Gans, D. O'Connell, Z. Lj. Petrovic, and T. Makabe, J. Phys. D **42**, 145206 (2009).
[5]T. Kimura and H. Kasugai, J. Appl. Phys. **108**, 033305 (2010).
[6]T. Czerwiec, F. Greer, and D. B. Graves, J. Phys. D **38**, 4278 (2005).
[7]K. Tao, D. Mao, and J. Hopwood, J. Appl. Phys. **91**, 4040 (2002).
[8]K. Ishikawa, Y. Yamaoka, M. Nakamura, Y. Yamazaki, S. Yamasaki, Y. Ishikawa, and S. Samukawa, J. Appl. Phys. **99**, 083305 (2006).
[9]N. Itagaki, S. Iwata, K. Muta, A. Yonesu, S. Kawakami, N. Ishii, and Y. Kawai, Thin Solid Films **435**, 259 (2003).
[10]W.-Y. Ding, J. Xu, W.-Q. Lu, X.-L. Deng, and C. Dong, Phys. Plasmas **16**, 053502 (2009).
[11]J. Amorim, H. S. Maciel, and J. P. Sudano, J. Vac. Sci. Technol. B **9**, 362 (1991).
[12]U. Kortshagen, N. D. Gibson, and J. E. Lawler, J. Phys. D **29**, 1224 (1996).
[13]S.-H. Seo, J.-I. Hong, K.-H. Bai, and H.-Y. Chang, Phys. Plasmas **6**, 614 (1999).
[14]M.-H. Lee, K. H. Lee, D.-S. Hyun, and C.-W. Chung, Appl. Phys. Lett. **90**, 191502 (2007).
[15]S. V. Singh, J. Appl. Phys. **103**, 083303 (2008).
[16]S. V. Singh and C. Pargmann, J. Appl. Phys. **104**, 083303 (2008).
[17]M. M. Turner and M. A. Lieberman, Plasma Sources Sci. Technol. **8**, 313 (1999).
[18]G. Cunge, B. Crowley, D. Vender, and M. M. Turner, Plasma Sources Sci. Technol. **8**, 576 (1999).
[19]S. Xu, K. N. Ostrikov, W. Luo, and S. Lee, J. Vac. Sci. Technol. A **18**, 2185 (2000).
[20]K. N. Ostrikov, S. Xu, and A. B. M. Shafiul Azam, J. Vac. Sci. Technol. A **20**, 251 (2002).

[21] J. Y. Bang, A. Kim, and C. W. Chung, Phys. Plasmas **17**, 064502 (2010).
[22] E. G. Thorsteinsson and J. T. Gudmundsson, Plasma Sources Sci. Technol. **18**, 045001 (2009).
[23] V. A. Godyak, *Soviet Radio Frequency Discharge Research* (Delphic, Falls Church, VA, 1986).
[24] J. T. Gudmundsson, T. Kimura, and M. A. Lieberman, Plasma Sources Sci. Technol. **8** 22 (1999).
[25] J.-H. Ku, Y.-K. Lee, and C.-W. Chung, Phys. Plasmas **17**, 043508 (2010).
[26] C. C. Hsu, M. A. Nierode, J. W. Coburn, and D. B. Graves, J. Phys. D **39**, 3272 (2006).
[27] J. Ma and Y. K. Pu, Phys. Plasmas **10**, 4118 (2003).
[28] H.-C. Lee, M.-H. Lee, and C.-W. Chung, Phys. Plasmas **17**, 013501 (2010).
[29] H.-C. Lee, J.-K. Lee, and C.-W. Chung, Phys. Plasmas **17**, 033506 (2010).
[30] C. W. Chung and H.-Y. Chang, Appl. Phys. Lett. **80**, 1725 (2002).
[31] H.-C. Lee, M.-H. Lee, and C.-W. Chung, Appl. Phys. Lett. **96**, 041503 (2010).
[32] D. Pagnon, J. Amorim, J. Nahorny, M. Touzeau, and M. Vialle, J. Phys. D **28**, 1856 (1995).
[33] M. A. Lieberman and A. J. Lichtenberg, *Principles of Plasma Discharge and Materials Processing* (Wiley, New York, 1994), p. 487.